An Adaptive Economic Model Predictive Control Approach for Wind Turbines

Mohamed L. Shaltout
Mem. ASME
Faculty of Engineering,
Mechanical Design and Production Department,
Cairo University,
Giza 12613, Egypt
e-mail: mshaltout@cu.edu.eg

Zheren Ma
Mem. ASME
Department of Mechanical Engineering,
University of Texas at Austin,
Austin, TX 78712
e-mail: zhrm@utexas.edu

Dongmei Chen
Mem. ASME
Department of Mechanical Engineering,
University of Texas at Austin,
Austin, TX 78712
e-mail: dmchen@me.utexas.edu

Motivated by the reduction of overall wind power cost, considerable research effort has been focused on enhancing both efficiency and reliability of wind turbines. Maximizing wind energy capture while mitigating fatigue loads has been one of the main goals for control design. Recent developments in remote wind speed measurement systems (e.g., light detection and ranging (LIDAR)) have paved the way for implementing advanced control algorithms in the wind energy industry. In this paper, an LIDAR-assisted economic model predictive control (MPC) framework with a real-time adaptive approach is presented to achieve the aforementioned goal. First, the formulation of a convex optimal control problem is introduced, with linear dynamics and convex constraints that can be solved globally. Then, an adaptive approach is proposed to reject the effects of model-plant mismatches. The performance of the developed control algorithm is compared to that of a standard wind turbine controller, which is widely used as a benchmark for evaluating new control designs. Simulation results show that the developed controller can reduce the tower fatigue load with minimal impact on energy capture. For model-plant mismatches, the adaptive controller can drive the wind turbine to its optimal operating conditions while satisfying the optimal control objectives. [DOI: 10.1115/1.4038490]

1 Introduction

The continuous growth in energy demand alongside environmental concerns has led to an immense need for clean and sustainable energy sources. One of the most abundant, renewable, and clean energy sources that can potentially satisfy future energy demand is the wind [1]. Consequently, the installation of wind turbines for power generation has grown rapidly worldwide during the last few decades [2]. For instance, the U.S. Department of Energy has set a goal of reaching a wind capacity level of 305 GW or 20% of the anticipated electrical power supply by the year 2030 [3]. However, the cost associated with wind energy generation has hindered the ambitious plans for installing more wind turbines. This challenge motivates significant research efforts to improve both efficiency and reliability of wind turbines, which ultimately leads to the reduction of wind energy cost.

Development of advanced control algorithms for wind turbines represents one of the major research areas that experiences extensive investigation [4,5]. Among different control methodologies, model predictive control (MPC) [6–8] has been explored to achieve specific objectives such as wind energy capture maximization, fatigue load mitigation, and wind power smoothing [9,10]. In a standard MPC, optimal steady-state set-points are first selected by an information management system through optimizing the economic costs of the plant operation. Then, through optimizing a tracking cost function, the MPC tracks such set-points while directly handling constraints on both inputs and states. The separation of the economic cost optimization and the optimal tracking controller undermines the overall performance whenever the operating plant deviates from its predefined set-point [11].

In order to improve the dynamic economic performance of the control system, economic MPC approach has been developed [11–13]. Unlike standard MPC that takes two steps to find the optimal solution, an economic MPC combines the information management system and set-points tracking into a single economic cost optimization step. Thus, the control system directly and dynamically optimizes the economic cost function online [11,14,15]; hence, the MPC gains its "economic" attribute. The economic MPC has recently been considered in numerous applications such as power systems [16], building climate control [17], and wind energy applications [18–22]. However, in order to successfully implement economic MPC for wind turbine control, several issues should be addressed.

An issue associated with MPC methodology is the requirement of an accurate turbine model. Conventionally, a low-order nonlinear model or a linearized model is adopted [23–25]. A comparison between linear and nonlinear MPCs in Ref. [26] shows that nonlinear MPC achieves better results when operating away from the linearization points of the linear MPC. However, implementing the nonlinear MPC yields a nonconvex optimal control problem that requires expensive computational effort to solve with no guarantee of a global optimal solution. In order to avoid this issue, nonlinear wind turbine dynamics and operating constraints are convexified without losing important information. As a result, convex optimal control algorithms can be used to yield a globally optimal solution.

As shown in Ref. [19], the optimal control problem within the economic MPC framework has been formulated as a convex optimal control problem with linear dynamics and convex constraints. It effectively smoothens the wind power supplied to the grid for an integrated turbine and energy storage system. Yet, this method does not consider the effect of control actions on turbine fatigue loading, which can cause premature failures. A more comprehensive control is desirable to optimize wind power supply as well as turbine fatigue mitigation. How to formulate the fatigue load estimation into a convex problem and minimize its associated computational cost are new challenges and will be discussed in this paper.

Moreover, standard MPC algorithms adopted for wind turbines assume the absence of model-plant mismatches. With this assumption, the standard MPC methodology usually achieves the anticipated objectives including smoothing wind power in Ref. [10], reducing fatigue loads in Refs. [23] and [27], and handling hard constraints on actuators in Ref. [28]. However, the

Contributed by the Dynamic Systems Division of ASME for publication in the Journal of Dynamic Systems, Measurement, and Control. Manuscript received February 16, 2017; final manuscript received November 9, 2017; published online December 19, 2017. Assoc. Editor: Ryozo Nagamune.

unmodeled aeroelastic response of the turbine blades and the stochastic nonuniform wind inflow introduce mismatches between the model and the plant parameters [29], which lead to degradation of the controller's performance. Many robust MPC algorithms [30,31] found in literature can handle model-plant mismatches. However, these algorithms focus on the uncertainty of wind speed measurement that affects the accuracy of the linearized model within the MPC framework. Alongside robust MPC algorithms, many adaptive control algorithms have been developed to reject the influence of other model uncertainties [32–35], such as changes in the blade aerodynamics over time which leads to deviations between the actual and theoretical power coefficient surfaces. Despite their success, those adaptive control algorithms need to evaluate the average system performance over a long-time horizon before adapting the control gains in real time. In addition, the tuning range of the control gains is large and may vary significantly for different wind turbines. Consequently, the adaptation rates of those algorithms are slow. A fast adaptive control algorithm was proposed by Ma et al. [36,37] and will be implemented here. It can rapidly and robustly track the optimal operating point that leads to maximum power generation under model uncertainties.

This paper describes the development of a light detection and ranging (LIDAR)-assisted economic MPC framework with an adaptive control for wind turbines. A wind turbine model is presented, including both drivetrain and tower fore-aft dynamics. Based on this model, an economic MPC controller is proposed using convex optimization approach. An LIDAR system is adopted to provide the necessary preview of wind speed ahead of the wind turbine. An adaptive algorithm is introduced to overcome model-plant mismatches. The developed controller maximizes wind energy capture and mitigates fatigue loads acting on the wind turbine tower while rejecting the effect of model-plant mismatches. The performance of the proposed framework is compared to a baseline controller (BLC) developed in Ref. [38], which incorporates a variable-speed generator torque control and a gain-scheduled proportional–integral blade pitch control.

The main contributions of this work are summarized as follows: First, the tower fore-aft dynamics is integrated into the convex optimal control problem, within the economic MPC framework, which can be solved globally. Second, the LIDAR-assisted economic MPC framework is applied to maximize energy capture and mitigate the tower fatigue loading for the full range of the wind turbine operation. Finally, an adaptive algorithm, developed previously by Ma et al. [36,37], is integrated into the economic MPC framework to robustly account for the model-plant mismatches.

2 Wind Turbine Model

A high-order nonlinear model of a horizontal axis wind turbine is selected as the plant model to carry out the numerical simulations [39]. However, the inclusion of such complex model within the economic MPC framework is not recommended due to the associated high computational cost. As a result, the high-order model is reduced to a lower order model, which is suitable for model-oriented control design. The models formulated in this section were introduced previously by the authors in Ref. [22] and presented here with more details for the review purpose.

2.1 Wind Power Plant Model. An eighth-order dynamic model of a wind turbine is presented here as the plant model [39]. It is based on the NREL 5 MW wind turbine model with its parameters summarized in Table 1 [38]. The wind turbine model consists of a third-order drivetrain model, a second-order tower model, a first-order generator model, and a second-order pitch actuator model. The third-order drivetrain model can be described as two rotating inertias connected with a torsional spring and damper

Table 1 NREL 5 MW wind turbine model parameters [38]

Parameter	Magnitude
Rated power, $P_{\text{g,rated}}$	5 MW
Rotor diameter, D_{r}	126 m
Hub height, H_{h}	90 m
Cut-in wind speed	3 m/s
Cut-out wind speed	25 m/s
Rated wind speed	11.4 m/s
Gear ratio, n	97
Rotor inertia, J_{r}	35,444,067 kg/m^2
Generator inertia, J_{g}	534.116 kg/m^2
Tower equivalent mass, M_{T}	438,000 kg
Tower equivalent damping, C_{T}	6421 N s/m
Tower equivalent stiffness, K_{T}	1,846,000 N/m
Optimal tip-speed ratio, λ^{o}	7.6
Optimal blade pitch angle, β^{o}	0 deg
Maximum power coefficient, $c_{\text{p,max}}$	0.4868

$$\dot{\omega}_r = \frac{1}{J_r}\left[T_r - \phi K_s - \dot{\phi} B_s\right]$$

$$\dot{\omega}_g = \frac{1}{J_g}\left[-T_g + \frac{1}{n}\left(\phi K_s + \dot{\phi} B_s\right)\right]$$

$$\dot{\phi} = \omega_r - \frac{1}{n}\omega_g$$

where ω_r, ω_g, and ϕ are the rotor speed, generator speed, and drivetrain torsional deflection, respectively. The rotor and generator inertias are denoted by J_r and J_g, respectively. The rotor and generator torques are denoted by T_r and T_g, respectively. The drivetrain equivalent torsional stiffness and damping are denoted by K_s and B_s, respectively. The gearbox ratio is denoted by n. The second-order tower model will be described in Sec. 2.2.

2.2 Reduced-Order Nonlinear Model. The eighth-order nonlinear model has been simplified to capture the relevant system dynamics that is crucial to the performance of the model predictive controller. The third-order drivetrain model has been reduced to single-order model, while the second-order model of the tower is kept the same. Both generator and pitch actuator models have been omitted. Thus, a third-order model is employed within the MPC framework. The dynamics of the wind turbine drivetrain can be described as a single rotational mass model as follows:

$$\dot{\omega}_g = \frac{1}{J}\left[\frac{1}{n}T_r - T_g\right] \tag{1}$$

with $\omega_g = n\omega_r$. The equivalent moment of inertia of both the rotor and generator calculated about the generator shaft (high-speed shaft) axis is given by $J = J_g + J_r/n^2$. Upper and lower bounds limit the generator speed and torque as follows:

$$\omega_{g,\min} \le \omega_g \le \omega_{g,\max} \tag{2a}$$

$$0 \le T_g \le T_{g,\max} \tag{2b}$$

The aerodynamic rotor torque includes one of the model nonlinearities and is calculated as follows:

$$T_r = \frac{1}{2\omega_r}\rho A c_p(\lambda, \beta) v^3 \tag{3}$$

where ρ is the air density, A is the rotor swept area, v is the wind speed, and β is the blade pitch angle. The tip-speed ratio $\lambda = \omega_r D_r/(2v)$, where D_r is the rotor diameter. The power

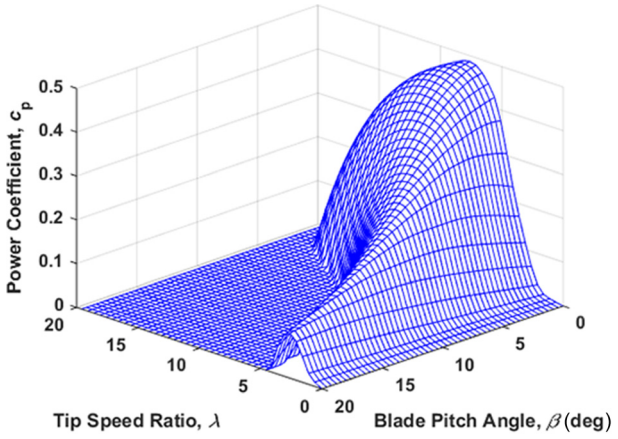

Fig. 1 Power coefficient of the NREL 5 MW horizontal axis wind turbine

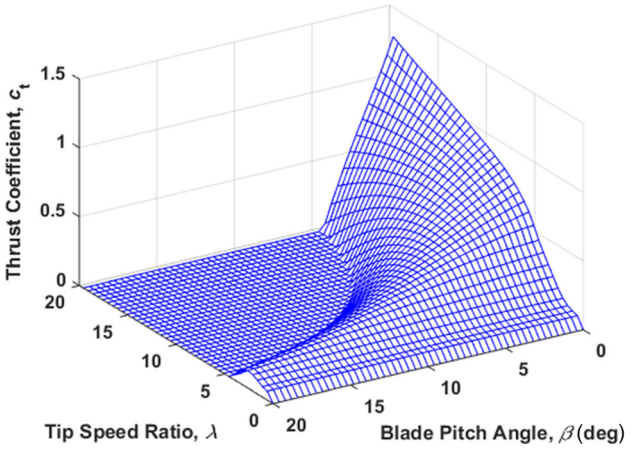

Fig. 2 Thrust coefficient of the NREL 5 MW horizontal axis wind turbine

coefficient c_p is a nonlinear function of the tip-speed ratio and blade pitch angle, which is shown in Fig. 1 and available as a lookup table. Upper and lower bounds limit the blade pitch angle as follows:

$$\beta_{\min} \le \beta \le \beta_{\max} \tag{4}$$

Finally, the aerodynamic power extracted from the wind by the rotor is given as

$$P_r = T_r \omega_r = \frac{1}{2}\rho A c_p(\lambda, \beta) v^3 \tag{5}$$

while the electrical generator power is given by

$$P_g = \eta_g T_g \omega_g \tag{6}$$

where η_g is the generator efficiency. The electrical generator power is limited by upper and lower bounds as follows:

$$0 \le P_g \le P_{g,\text{rated}} \tag{7}$$

where $P_{g,\text{rated}}$ is the rated generator power.

The dynamics of the fore-aft bending mode of the tower is modeled as a second-order system [40]

$$M_T \ddot{x}_T + B_T \dot{x}_T + K_T x_T = F_T \tag{8}$$

where x_T is the fore-aft displacement of the tower top, and M_T, B_T, and K_T are the tower equivalent mass, structural damping, and bending stiffness, respectively. The thrust force F_T, which includes another model nonlinearity, is calculated as follows:

$$F_T = \frac{1}{2}\rho A c_t(\lambda, \beta) v^2 \tag{9}$$

where the thrust coefficient c_t is a nonlinear function of the tip-speed ratio and blade pitch angle, which is shown in Fig. 2 and also available as a lookup table.

The reduced-order nonlinear model of the wind turbine drivetrain and tower (i.e., Eqs. (1) and (8)) can be rearranged in a standard nonlinear state-space form

$$\dot{\mathbf{x}} = f(\mathbf{x}, \mathbf{u}, d)$$

$$\mathbf{y} = g(\mathbf{x}, \mathbf{u}, d)$$

where the state vector $\mathbf{x}$, the input vector $\mathbf{u}$, the disturbance d, and the output vector $\mathbf{y}$ are

$$\begin{cases} \mathbf{x} = [\omega_g \; x_T \; \dot{x}_T]^{\mathrm{T}} \\ \mathbf{u} = [T_g \; \beta]^{\mathrm{T}} \\ d = v \\ \mathbf{y} = [\omega_g \; x_T \; \dot{x}_T]^{\mathrm{T}} \end{cases} \tag{10}$$

3 Formulation of the Convex Optimization Problem

The integration of convex optimization tools within a model predictive control framework requires the transformation of the aforementioned nonlinear model to a new model with linear dynamics and convex constraints [19]. The concept behind this transformation is to visualize the drivetrain model of the wind turbine from the perspective of power flows and energies. The convex optimization problem formulated in this section was introduced previously in Ref. [22] and presented here with more details for the review purpose.

This model consists of a turbine drivetrain model and a tower model. The model variables described in Eq. (10) are transformed to a set of new variables as follows:

$$\begin{cases} \mathbf{x} = [K \; X \; V]^{\mathrm{T}} \\ \mathbf{u} = [P_g \; P_r]^{\mathrm{T}} \\ d = v \\ \mathbf{y} = [K \; X \; V]^{\mathrm{T}} \end{cases} \tag{11}$$

where K is the kinetic energy stored in the rotating components (i.e., $K = (J/2)\omega_g^2$), and X and V are the displacement and velocity of the tower top as a function of the new variables, respectively. The transformation from the original set of variables to the new set of variables, and vice versa, will be detailed in this section. For instance, the generator torque can be reconstructed from the new variables (i.e., P_g and K) as follows:

$$T_g = \frac{P_g}{\omega_g \eta_g} = \frac{P_g}{\eta_g \sqrt{2K/J}}$$

3.1 Drivetrain Dynamic Model. Using the new set of variables, the drivetrain dynamics in Eq. (1) can be transformed as follows:

$$\dot{K} = J\omega_g \dot{\omega}_g = \omega_g \left(\frac{1}{n} T_r - T_g\right) = P_r - \frac{1}{\eta_g} P_g \tag{12}$$

The constraints defined in Eq. (2) can be rewritten as follows:

$$\frac{J}{2}\omega_{g,\min}^2 \le K \le \frac{J}{2}\omega_{g,\max}^2 \tag{13a}$$

$$0 \le P_g \le \eta_g T_{g,\max}\sqrt{2K/J} \tag{13b}$$

where Eq. (13*a*) is a linear constraint on K, and Eq. (13*b*) is a convex constraint on P_g and K, where $\sqrt{2K/J}$ is a concave function of K.

A new variable called the available wind power is defined as a function of kinetic energy and wind speed as follows:

$$P_{\text{av}}(v,K) = \max_{\beta_{\min}\le\beta\le\beta_{\max}} \frac{1}{2}\rho A c_p\left(v, \frac{1}{n}\sqrt{2K/J}, \beta\right)v^3 \tag{14}$$

As can be seen from Eq. (14), the tip-speed ratio inside the power coefficient function has been replaced by wind speed and kinetic energy. Thus, the lookup table of the power coefficient can be rebuilt as a function of wind speed, kinetic energy, and blade pitch angle. Consequently, a new lookup table for the available wind power can be constructed based on the original lookup table of the power coefficient. For a given wind speed and kinetic energy (i.e., generator speed), the available wind power represents an upper bound on the aerodynamic power extracted from the wind by the rotor as follows:

$$0 \le P_r \le P_{\text{av}}(v,K) \tag{15}$$

According to Eq. (15), as the blade pitch angle β varies, the extracted power P_r increases from zero to the available power $P_{\text{av}}(v,K)$ at given values of wind speed and kinetic energy. As a result, the blade pitch angle can be inversely calculated with the knowledge of wind speed, kinetic energy, and extracted power.

The next step is to establish the convexity of the constraint defined in Eq. (15). The variation of the available power $P_{\text{av}}(v,K)$, normalized by v^3, with the kinetic energy K for different wind speeds is shown in Fig. 3. It can be noticed that for each wind speed, the normalized available power $P_{\text{av}}(v,K)/v^3$ is nearly a concave function of kinetic energy K. Consequently, it is possible to approximate $P_{\text{av}}(v,K)$ for each wind speed as a concave function of K with relatively small error (less than 1%).

In Ref. [19], the approximated available power is computed for a number of discrete values v_i of the wind speed and expressed as piecewise linear functions as follows:

$$\hat{P}_{\text{av},v_i}(K) = \min\{a_1K + b_1, \ldots, a_kK + b_k\}v_i^3$$

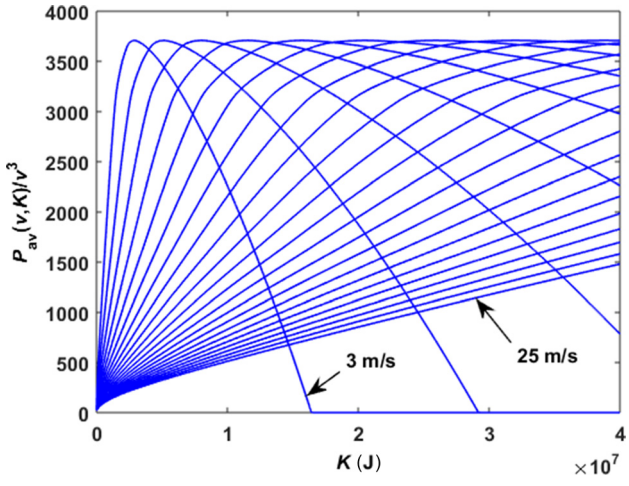

Fig. 3 The available power $P_{\text{av}}(v,K)$ normalized by v^3 and plotted against kinetic energy K for a range of wind speeds from 3 m/s to 25 m/s with an increment of 1 m/s

with k affine functions [41]. For any value of wind speed, v lies between two discrete values v_1 and v_2, it is possible to find the approximation $\hat{P}_{\text{av}}(v,K)$ of the available power $P_{\text{av}}(v,K)$ by linear interpolation of two adjacent functions $\hat{P}_{\text{av},v_1}(K)$ and $\hat{P}_{\text{av},v_2}(K)$

$$\hat{P}_{\text{av}}(v,K) = (1-\epsilon)\hat{P}_{\text{av},v_1}(K) + \epsilon\hat{P}_{\text{av},v_2}(K) \tag{16}$$

where $\epsilon = (v - v_1)/(v_2 - v_1)$. The approximated available power $\hat{P}_{\text{av}}(v,K)$ is a concave function of K because it is a linear interpolation of two concave functions. As a result, the constraint defined in Eq. (15) can be replaced, with negligible error, by the following convex constraint:

$$0 \le P_r \le \hat{P}_{\text{av}}(v,K) \tag{17}$$

3.2 Tower Dynamic Model. The dynamics of the fore-aft bending mode of the tower described in Eq. (8) can be rewritten in a state-space form as a function of the new variables as follows:

$$\begin{cases} \dot{X} = V \\ \dot{V} = \dfrac{1}{M_T}[F_T(v,K,P_r) - B_T V - K_T X] \end{cases} \tag{18}$$

Based on the new variable transformation, the nonlinear thrust force F_T is formulated as a function of wind speed, kinetic energy, and aerodynamic rotor power. As previously mentioned, formulation of the convex optimization problem requires a model with linear dynamics and convex constraints. At each time-step, the nonlinear thrust force in Eq. (18) will be replaced with a linear approximation to yield a linear dynamic model. Consequently, a convex optimization problem can be solved globally and rapidly instead of using computationally expensive nonconvex optimization tools.

For the model predictive control algorithm, the measured wind speed profile over the prediction horizon is available at the beginning of the algorithm execution. Additionally, new measurements of generator speed (i.e., kinetic energy) and blade pitch angle are also available. With the knowledge of the wind speed at each time-step, the power and thrust coefficients can be represented as nonlinear functions of the kinetic energy and blade pitch angle

$$c_p^i(K,\beta) = \frac{P_r^i}{0.5\rho A v_i^3} \tag{19a}$$

$$c_t^i(K,\beta) = \frac{F_T^i}{0.5\rho A v_i^2} \tag{19b}$$

where $i = \{1,2,\ldots,N_p\}$, and N_p is the prediction and control horizon. For each wind speed, the maximum thrust force can be defined as

$$F_T^i = \max_{\substack{\beta_{\min}\le\beta\le\beta_{\max}\\ K_{\min}\le K\le K_{\max}}} 0.5\rho A c_t(K,\beta)v_i^2$$

Then, the linearization procedure starts with performing first-order Taylor series expansions of the power and thrust coefficients around the measured kinetic energy K^* and blade pitch angle β^* as follows:

$$c_p^i(k,\beta) = c_p^i(K^*,\beta^*) + \left.\frac{\partial c_p^i}{\partial K}\right|_{K^*,\beta^*}(K^i - K^*) + \left.\frac{\partial c_p^i}{\partial \beta}\right|_{K^*,\beta^*}(\beta^i - \beta^*)$$
$$= q_p^i\beta^i + r_p^iK^i + s_p^i \tag{20a}$$

$$c_t^i(k,\beta) = c_t^i(K^*,\beta^*) + \left.\frac{\partial c_t^i}{\partial K}\right|_{K^*,\beta^*}(K^i - K^*) + \left.\frac{\partial c_t^i}{\partial \beta}\right|_{K^*,\beta^*}(\beta^i - \beta^*)$$
$$= q_t^i\beta^i + r_t^i K^i + s_t^i \tag{20b}$$

where q_p^i, r_p^i, s_p^i, q_t^i, r_t^i, and s_t^i are constants and can be directly derived from Eq. (20) for each step of the prediction horizon. Combining Eqs. (19) and (20) and eliminating the blade pitch angle β^i, a linear relationship between thrust force from one side and rotor power and kinetic energy from the other side can be derived at each time-step

$$\hat{F}_T^i = \left(\frac{q_t^i}{q_p^i v_i}\right)P_r^i + 0.5\rho A v_i^2\left(r_t^i - r_p^i\frac{q_t^i}{q_p^i}\right)K^i + 0.5\rho A v_i^2\left(s_t^i - s_p^i\frac{q_t^i}{q_p^i}\right)$$
$$= Q^i P_r^i + R^i K^i + S^i \tag{21}$$

The linear expression in Eq. (21) can be rearranged in a compact matrix form as follows:

$$\hat{\mathbf{F}}_T = \mathbf{Q}P_r + \mathbf{R}K + \mathbf{S} \tag{22}$$

with

$$0 \le \hat{\mathbf{F}}_T \le \mathbf{F}_{T,\max}$$

where $\hat{\mathbf{F}}_T$ is the linearized thrust force vector corresponding to the measured wind speed vector as a function of the new variables, $\mathbf{Q} = \mathrm{diag}(Q^i)$ is an $N_p \times N_p$ matrix, $\mathbf{R} = \mathrm{diag}(R^i)$ is an $N_p \times N_p$ matrix, $\mathbf{S} = \left[S^1,\ldots,S^{N_p}\right]^{\mathrm{T}}$ is an $N_p \times 1$ vector, and $\mathbf{F}_{T,\max} = \left[F_{T,\max}^i,\ldots,F_{T,\max}^{N_p}\right]^{\mathrm{T}}$ is an $N_p \times 1$ vector. Finally, the nonlinear thrust force in Eq. (18) will be replaced with the linear expression derived in Eq. (22), thus yielding a linear tower dynamic model as a function of the new variables.

This linear approximation is repeated at each time-step with new measurements of wind speed, generator speed, and blade pitch angle. The error between the linear and nonlinear thrust forces depends mainly on the accuracy of the measured wind speed and the deviation of generator speed and blade pitch angle during the prediction horizon from their initial measured values. The previously mentioned linearization method provides a prediction of the thrust force leading to a linear wind turbine model (i.e., drivetrain and tower). Consequently, the convex optimization problem within the economic MPC can be globally solved with significantly lower computational effort compared to nonlinear MPC approaches [23].

3.3 Convex Optimization Problem. The analysis in Secs. 3.1 and 3.2 has detailed the linearization of the nonlinear wind turbine model using the new variables transformation defined in Eq. (11) as follows:

$$\begin{cases}\dot{K} = P_r - \dfrac{1}{\eta_g}P_g \\ \dot{X} = V \\ \dot{V} = \dfrac{1}{M_T}[QP_r + RK + S - B_T V - K_T X]\end{cases} \tag{23a}$$

The linearized wind turbine model can be directly represented in a standard linear state-space form as follows:

$$\dot{\mathbf{x}}(t) = \mathbf{A}_t\mathbf{x}(t) + \mathbf{B}_t\mathbf{u}(t) \tag{23b}$$

where $\mathbf{A}_t \in \mathbb{R}^{3\times3}$ and $\mathbf{B}_t \in \mathbb{R}^{3\times2}$ are the system and input matrices, respectively. Additionally, the linearized wind turbine model is subjected to the convex constraints defined in Eqs. (13) and (17) on the state K and the inputs P_r and P_g

$$\begin{cases}\dfrac{J}{2}\omega_{g,\min}^2 \le K \le \dfrac{J}{2}\omega_{g,\max}^2 \\ 0 \le P_g \le \min\left\{\eta_g T_{g,\max}\sqrt{2K/J}, P_{g,\text{rated}}\right\} \\ 0 \le P_r \le \hat{P}_{\text{av}}(v,K) \\ 0 \le \hat{F}_T \le F_{T,\max}\end{cases} \tag{24}$$

As previously mentioned, the main goal of solving this convex optimization problem is to find the optimal control inputs (i.e., P_g and P_r) that satisfy two main objectives, namely, maximization of power generation and minimization of tower fatigue loads. The cost function E is defined as the integral of the objective function F over the time horizon T while considering the linear model defined in Eq. (23*b*) and the set of constraints G defined in Eq. (24)

$$\begin{aligned}&\max_{u(t)}\ E = \int_0^T F(x(t),u(t),d(t))dt, \quad \forall t \in [0,T] \\ &\text{s.t.}\quad \dot{\mathbf{x}}(t) = \mathbf{A}_t\mathbf{x}(t) + \mathbf{B}_t\mathbf{u}(t) \\ &\qquad \mathbf{x}(0) = \mathbf{x}_0 \\ &\qquad G(\mathbf{x}(t),\mathbf{u}(t),d(t)) \ge 0\end{aligned} \tag{25}$$

The objective function F is constructed from a number of terms as follows:

$$F(x(t),u(t),d(t)) = \alpha_1 P_g(t) - \alpha_2\left[\dot{P}_g(t)\right]^2 - \alpha_3\left[\dot{P}_r(t)\right]^2 + \alpha_4\hat{P}_{\text{av}}(v(t),K(t)) - \alpha_5[V(t)]^2 - \alpha_6\left[\max\left\{K(t) - \frac{J}{2}\omega_{g,\text{rated}}^2, 0\right\}\right] - \alpha_7\left[K(t) - \bar{\mathbf{K}}\right]^2 \tag{26}$$

where α_1–α_7 are the positive constants that determine the tradeoffs among the objective function terms. In order to solve the optimal control problem as a convex optimal control problem, it is essential to prove the concavity (i.e., convexity for minimization) of all the terms of the cost function. The positive terms of the cost function will be maximized, while the negative terms will be minimized.

The first term represents the total energy harvested over a period of time T, which is a linear (concave) function of the control input P_g. The second term represents the variation of the generated power over time, which is a quadratic (convex) function. The third term represents the variation of the rotor power over time, which is a quadratic (convex) function. The fourth term represents the approximated available wind power, which was proven to be concave in Eq. (16). The fifth term is the velocity of the tower top, which is a quadratic (convex) function. Here, the basic strategy is to minimize the fatigue loads acting on the tower base due to the variations of the tower fore-aft bending moment (TFAM), which is calculated as follows [23]:

$$\frac{d}{dt}(\text{TFAM}) = H_h(B_T\ddot{x}_T + K_T\dot{x}_T)$$

where H_h is the hub height. Thus, directly minimizing the rate of change of the fore-aft bending moment will eventually minimize

$\ddot{x}_T$ causing the undesirable minimization of x_T which is not effective in fatigue load mitigation. Consequently, minimizing $\dot{x}_T$ only will effectively minimize the rate of change of the fore-aft bending moment, hence, mitigate the fatigue loads. The sixth term is a penalty on the kinetic energy (i.e., generator speed) for exceeding its rated value, which is a convex function.

The last term is the deviation of the kinetic energy away from its reference value, which is a quadratic (convex) function. The reference kinetic energy $\bar{\mathbf{K}}$ is determined by

$$\bar{\mathbf{K}} = 2J\left(\frac{nv}{D_r}\right)^2(\lambda^*)^2$$

where λ^* is the reference tip-speed ratio. Ideally, the reference tip-speed ratio is equivalent to the theoretical optimal tip-speed ratio (i.e., $\lambda^* = \lambda^o$). However, the existence of model-plant mismatches leads to the deviation of the optimal tip-speed ratio from its theoretical value due to blade deflection, nonuniform wind inflow, etc. Consequently, an adaptive approach is adopted to search for the true optimal tip-speed ratio during wind turbine operation. Thus, the last term in the objective function Eq. (26) will ensure the convergence of the reference tip-speed ratio to the true optimal tip-speed ratio. The adaptive approach algorithm will be detailed in Sec. 4. Finally, the optimal control problem can be solved globally as a convex optimal control problem, with linear dynamics, convex constraints, and concave objective function to be maximized.

4 Control Methodology

The proposed control framework integrates an LIDAR-assisted economic model predictive controller (eMPC) with an adaptive algorithm to maximize wind energy capture and mitigate the tower fatigue loads while rejecting the effects of model-plant mismatches. A block diagram of the proposed control design is shown in Fig. 4. The details of the eMPC and the adaptive algorithm are presented in Secs. 4.1 and 4.2.

4.1 Light Detection and Ranging-Assisted Economic Model Predictive Control. The effective implementation of the eMPC requires a preview information of the wind disturbances ahead of the wind turbine. In this paper, an LIDAR system [42–44] is used to provide a perfect preview of the hub-height wind speed over a prediction horizon $T = 10$s with an update rate $\Delta t = 0.2$s equivalent to the LIDAR update rate [23]. The wind speed direction is assumed to be unchanging and facing the rotor plan. As a result, the prediction horizon (same as the control horizon) can be divided into $N_p = 50$ steps. Consequently, a discretized optimal control problem, equivalent to Eq. (25), is solved over the prediction horizon at each step

$$\begin{aligned} \max_{u(i)} \quad & E = \sum_{i=0}^{N_p-1} F\big(x(i), u(i), d(i)\big) \\ \text{s.t.} \quad & \mathbf{x}(i+1) = \mathbf{A}_d\mathbf{x}(i) + \mathbf{B}_d\mathbf{u}(i) \\ & \mathbf{x}(0) = \mathbf{x}_0 \\ & G\big(\mathbf{x}(i), \mathbf{u}(i), d(i)\big) \geq 0 \end{aligned} \tag{27}$$

where $\mathbf{A}_d \in \mathbb{R}^{3\times3}$ and $\mathbf{B}_d \in \mathbb{R}^{3\times2}$ are the discrete system and input matrices, respectively. A sequence of control inputs will be obtained from solving the optimal control problem in Eq. (27), out of which the control input at the first step $u(0)$ is applied to the plant. As a set of new measurements is available, the controller repetitively solves the optimal control problem in Eq. (27) at each step (i.e., equal to the LIDAR update rate).

4.2 Adaptive Approach. In addition to the previewed wind speed and the measured states, the eMPC also requires the true optimal tip-speed ratio. The optimal reference tip-speed ratio may deviate from the simulation-derived optimal value due to blade deflection, nonuniform wind inflow, etc. An adaptive algorithm, previously developed by Ma et al. [36], is recaptured as follows.

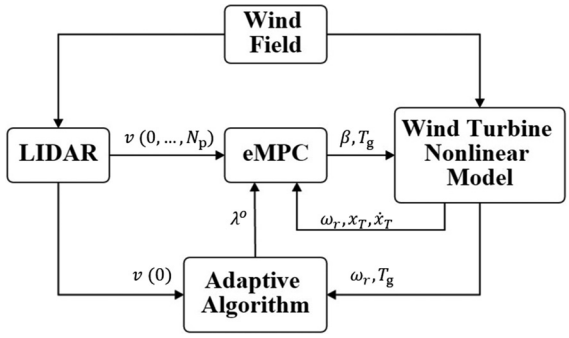

Fig. 4 A simplified block diagram of the wind turbine closed-loop system with the eMPC and the adaptive algorithm

In every T_{adp} seconds, the algorithm checks whether the tip-speed ratio has converged to its reference value based on the following condition:

$$\left|\lambda_{\text{avg}} - \lambda^*\right| < \delta \tag{28}$$

where λ_{avg} refers to the average tip-speed ratio during the time period T_{adp}, and δ is a small positive constant to test the convergence of the tip-speed ratio. If the previously mentioned condition is not satisfied, the algorithm proceeds without updating λ^*. Otherwise, the average power coefficient during this period is estimated as follows:

$$c_{p,\text{avg}} = \frac{0.5J_r\left(\omega_{r,f}^2 - \omega_{r,0}^2\right) + n\int_{t_0}^{t_f} T_g\omega dt}{0.5\rho A\int_{t_0}^{t_f} v^3 dt} \tag{29}$$

where t_0 and t_f denote the start and end times of the period; $\omega_{r,0}$ and $\omega_{r,f}$ are the rotor speed at t_0 and t_f, respectively. Then, λ_{avg} and $c_{p,\text{avg}}$ are recorded in sets Λ and Γ, respectively. Let $G_{n\times1}$ denotes the largest subset of Λ such that $|g_i - \lambda^o| < \delta$ is satisfied $\forall g_i \in G_{n\times1}$. $H_{n\times1}$ denotes a subset of Γ that corresponds to $G_{n\times1}$. An adaptive approach based on a local linear regression method is applied as follows:

$$\begin{cases} \lambda^o(k+1) = \lambda^o(k) + \eta sign[(G-\bar{G})^{\mathrm{T}}(H-\bar{H})] \\ \eta = \alpha\left|\left((G-\bar{G})^{\mathrm{T}}(G-\bar{G})\right)^{-1}(G-\bar{G})^{\mathrm{T}}(H-\bar{H})\right| \\ \eta_{\min} \leq \eta \leq \eta_{\max} \end{cases} \tag{30}$$

where $\bar{G}$ and $\bar{H}$ refer to the mean value of G and H, respectively, and α is an influence factor of the step size η. A lower-bound step size $\eta_{\min}$ is selected to prevent the adaptation rate from severely slowing down. The step size is also limited by an upper bound, $\eta_{\max}$, to minimize the effect of sudden measurement errors or disturbances on the wind turbine. The parameters to be selected in the proposed adaptive method include the length of the time period, T_{adp}, the step size influence factor, α, and the bounds on the step size, $\eta_{\min}$ and $\eta_{\max}$. This adaptive technique allows the eMPC to robustly converge to the optimal operation of a wind turbine system despite the model-plant mismatches.

5 Simulation Results

The performance of developed eMPC is compared to the performance of a BLC, which is widely used as a benchmark for evaluating new control algorithms. It combines a variable-speed generator torque controller and a gain-scheduled proportional–integral blade pitch

controller. Both controllers operate under the same constraint of maximum rate limits of the control inputs (i.e., blade pitch angle and generator torque). The main aspects of comparison are the efficiency of wind energy capture and TFAM. The damage equivalent load (DEL) represents a means for evaluating the TFAM acting on the turbine tower. It is a single number that quantitatively indicates the damage caused by fatigue loadings acting on wind turbine structure and drivetrain [45–47]. In this study, the TFAM DEL is obtained using a rainflow-counting algorithm with the NREL MLife code [48]. The first set of results shows responses of both controllers to step changes of wind speed. Next, responses of both controllers under volatile wind speed profiles are presented and compared. Finally, a model-plant mismatch is introduced to investigate its effect on the performance of both controllers.

5.1 Controller Performance Under Stepwise Wind Speed. A comparison between the responses of BLC and eMPC to step changes in wind speed ranging from 8 to 10 m/s is shown in Fig. 5. As shown in Fig. 5, the oscillations in the TFAM have been reduced significantly in case of eMPC as compared to BLC. Additionally, the TFAM DEL has been reduced by 6.6% as shown in Table 2. This improvement is attributed to the blade pitch control of the eMPC around the step change instance. This blade pitching activity is not possible in case of BLC because the blade pitch control is only active for above rated generator speed operation. The TFAM is mainly caused by the thrust force acting on the turbine rotor disk. As shown in Fig. 2, increasing the blade pitch angle leads to the decrease of the thrust coefficient, which eventually leads to the reduction of the thrust force. However, deviating the blade pitch angle away from its optimal value leads to slight reduction in power coefficient, which results in a 0.65% drop of wind energy capture.

Figure 6 compares the responses of BLC and eMPC to steps in wind speed ranging from 11 to 13 m/s, and the results are summarized in Table 3. With eMPC, a reduction of up to 26% is achieved in TFAM DEL with a slight sacrifice in energy capture (i.e., 0.29%). At time around 200 s, the wind turbine with LIDAR-assisted eMPC switches from partial-load to full-load operation. At that switching instant, it can be noticed that both generator power and torque gradually and smoothly shift from their steady-state values in the partial-load region to their rated steady-state values in the full-load region.

Table 2 Comparison between the performance of the BLC and eMPC under stepwise in wind speed

Controller	Energy (kW h)	TFAM DEL (MN m)
Steps in wind speed ranging from 8 to 10 m/s		
BLC	257.1420	29.106
eMPC	255.4699	27.173
eMPC versus BLC	−0.6502%	−6.6412%
Steps in wind speed ranging from 11 to 13 m/s		
BLC	516.7889	46.577
eMPC	515.2734	34.363
eMPC versus BLC	−0.2933%	−26.223%

5.2 Controller Performance Under Volatile Wind Speed Profiles. The next step in the investigation process of the eMPC effectiveness is to evaluate its response under volatile wind speed profiles. Two wind speed profiles were generated using TurbSim [49] with 25% turbulence intensity and average wind speeds equal to 7.5 and 12.5 m/s, respectively. Figure 7 shows a comparison between the responses of BLC and eMPC under a volatile wind profile with an average wind speed equal to 7.5 m/s. The quantitative comparison results are summarized in Table 3. A significant reduction, up to 25%, in the TFAM DEL has been achieved by using eMPC as compared to BLC with a slight loss in energy capture (i.e., 0.5%). The reduction in energy capture is mainly attributed to the blade pitching activity, as shown in Fig. 7, aiming at

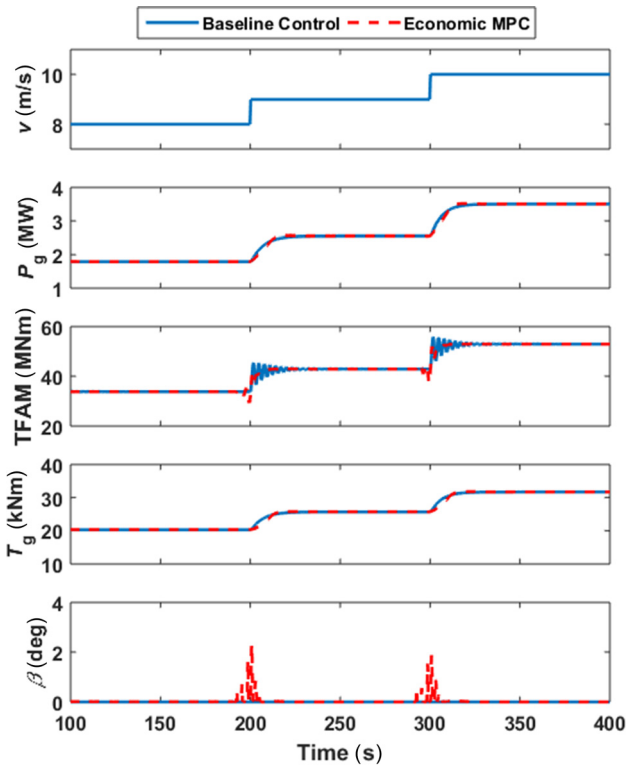

Fig. 5 A comparison between the responses of the BLC and the eMPC to steps in wind speed ranging from 8 to 10 m/s with 1 m/s increment

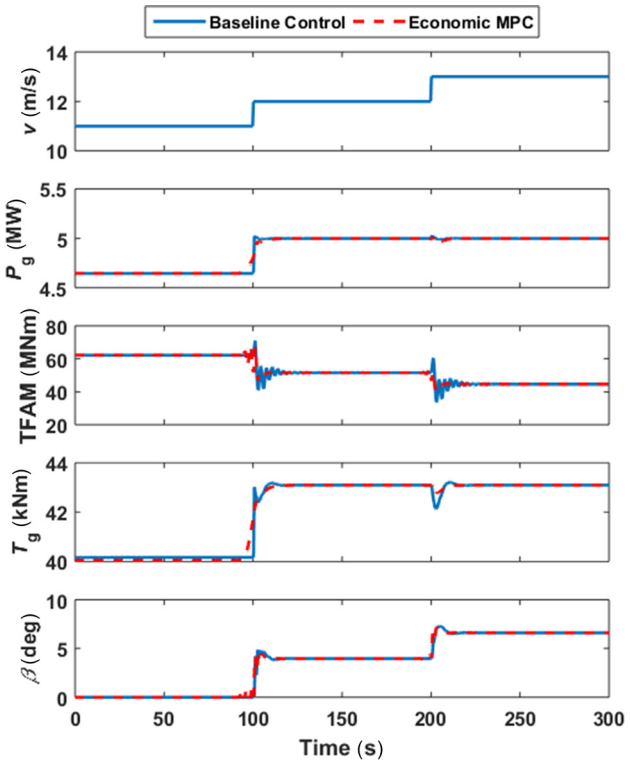

Fig. 6 A comparison between the responses of the BLC and the eMPC to steps in wind speed ranging from 11 to 13 m/s with 1 m/s increment

Table 3 Comparison between the performance of the BLC and eMPC under volatile wind speed profiles

Controller	Energy (kW h)	TFAM DEL (MN m)
Wind speed profile with 7.5 m/s mean wind speed		
BLC	259.4681	31.421
eMPC	258.1350	23.558
eMPC versus BLC	−0.5138%	−25.025%
Wind speed profile with 12.5 m/s mean wind speed		
BLC	760.9337	83.114
eMPC	769.8906	64.130
eMPC versus BLC	+1.1771	−22.8409%

reducing the TFAM DEL. As previously explained, deviating the blade pitch angle away from its optimal value during partial-load operation leads to a slight reduction in power coefficient, hence energy capture.

Figure 8 shows another comparison between the responses of BLC and eMPC under a volatile wind profile with an average wind speed equal to 12.5 m/s. The quantitative results summarized in Table 3 show an improvement in both energy capture by 1.17% and TFAM DEL by 22.8% for the eMPC as compared to BLC. Figure 8 also shows the significant reduction in the sudden variations of the control actions, namely, the generator torque and the blade pitch angle, in case of eMPC as compared to BLC. This is attributed to the effect of the second and third terms in the cost function (Eq. (26)).

For both wind speed profiles, the results in Tables 2 and 3 agree with results obtained in Ref. [23], which adopted a nonlinear model predictive control approach. The results showed the improvement of TFAM DEL for wind profiles with average wind speeds below 8 m/s and the improvement of both energy capture and TFAM DEL for average wind speeds above 8 m/s.

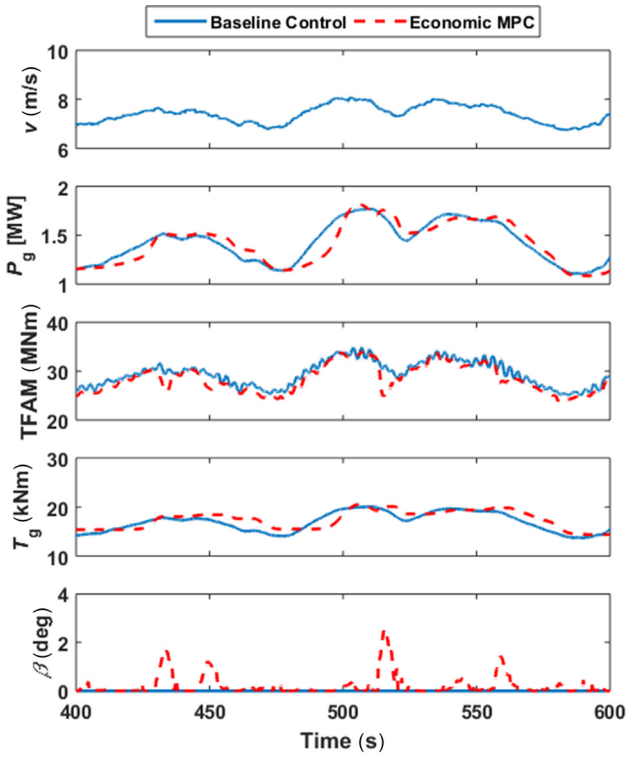

Fig. 7 A comparison between the responses of the BLC and the eMPC under a 10 min volatile wind profile with an average equal to 7.5 m/s

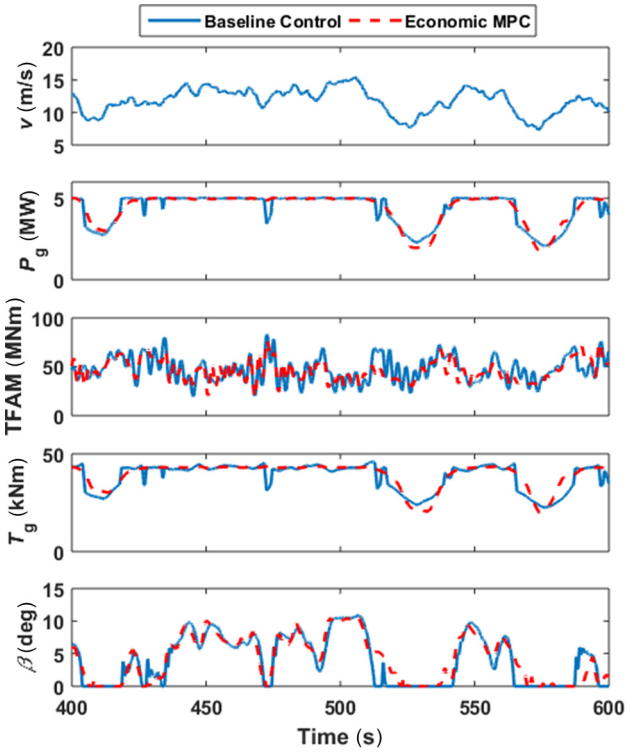

Fig. 8 A comparison between the responses of the BLC and the eMPC under a 10 min volatile wind profile with an average equal to 12.5 m/s

5.3 Controller Performance Under Model-Plant Mismatches. In the previously mentioned results, the model parameters were assumed to perfectly match the plant parameters. In this subsection, the impact of model-plant mismatch on the responses of BLC and eMPC with the proposed adaptive approach is investigated. As previously mentioned, the most important parameter of a wind turbine is its power coefficient, which is a function of the tip-speed ratio and blade pitch angle. The aforementioned model-plant mismatches are mainly related to deviations between the actual and theoretical power coefficient surfaces. The impact of model-plant mismatches on controller performance is more significant during partial-load operation, as they directly affect the energy capture. Nevertheless, tracking the optimal tip-speed ratio is not an objective during full-load operation. Consequently, this subsection will focus only on the controller's response in the partial-load region.

During partial-load operation, the blade pitch angle is set at its optimal value in case of BLC. Concurrently, the generator torque control law takes the following form:

$$T_g = M\omega_g^2, \quad \text{with} \quad M = \frac{1}{16}\rho A D_r^3 \frac{c_p(\lambda^o)}{(\lambda^o)^3} \tag{31}$$

The torque control gain, M, depends on the optimal tip-speed ratio and the corresponding maximum power coefficient. Thus, a deviation of the optimal tip-speed ratio results in a deviated control gain. As a result, the BLC fails to track the actual optimal tip-speed ratio for maximum energy capture. In order to study the effect of deviations in the power coefficient from its theoretical value on the controller response, a deviated power coefficient surface $c_p^d(\lambda_d, \beta)$ is assumed as shown in Fig. 9. The introduced deviation leads to 10% error in the optimal tip-speed ratio (i.e., $\lambda_d^o = 0.9\lambda^o$) and the maximum power coefficient (i.e., $c_p^d(\lambda_d^o) = 1.1c_p(\lambda^o)$). A corresponding deviation has also been introduced to the thrust coefficient surface.

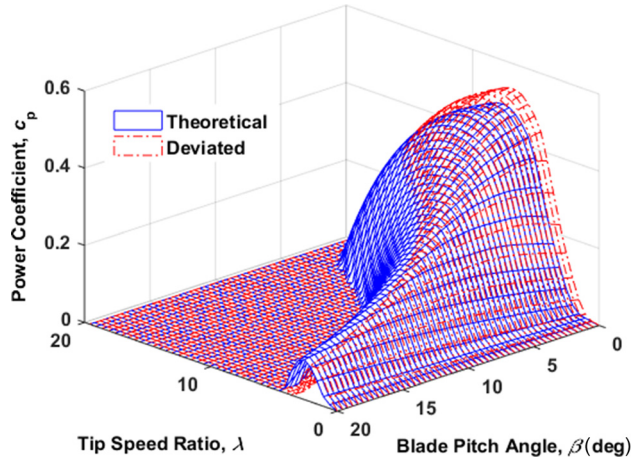

Fig. 9 Theoretical versus deviated power coefficient for the NREL 5 MW horizontal axis wind turbine

A wind speed profile with 25% turbulence intensity, 7.5 m/s average wind speed, and 20 min time span is used to demonstrate the response of both controllers under model-plant mismatches. As shown in Fig. 10, as the torque control gain deviates from its true optimal value, the BLC fails to track the actual optimal tip-speed ratio. Consequently, the BLC fails to maximize the power coefficient which leads to a drop in energy capture. On the other hand, the tip-speed ratio gradually converges to its actual optimal value in case of eMPC with the adaptive approach. This is attributed to the ability of the adaptive algorithm to update the reference tip-speed ratio despite the mismatches between the model and the plant parameters.

Consequently, the eMPC can achieve higher values of the power coefficient, hence energy capture. Additionally, the blade pitch angle activity in case of eMPC is mainly responsible for the significant decrease in TFAM DEL as shown in Table 4.

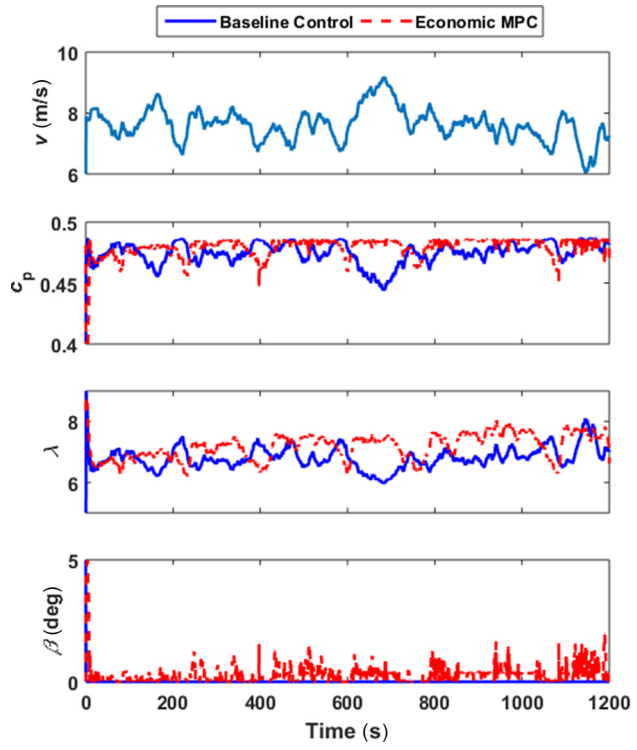

Fig. 10 A comparison between the responses of BLC and eMPC with model-plant mismatches under a 20 min volatile wind profile with an average equal to 7.5 m/s

Table 4 Comparison between the performance of the BLC and eMPC under model-plant mismatches

Controller	Energy (kW h)	TFAM DEL (MN m)
BLC	512.2372	29.318
eMPC	519.3657	23.061
eMPC versus BLC	+1.3916%	−21.34%

6 Conclusion

In this work, an LIDAR-assisted eMPC framework with an adaptive approach for wind turbines has been developed to maximize wind energy capture, reduce the tower fatigue loading, and reject the model-plant mismatch. Convex optimal algorithms have been used to find the global optimal controller. An adaptive algorithm has also been integrated with the eMPC framework to reject the effects of model-plant mismatches. Compared to the baseline controller, simulation results show that the proposed controller reduces tower fatigue load with a minimal impact on energy capture. Additionally, the adaptive algorithm proves its effectiveness in rejecting the impacts of model-plant mismatches on the controller performance. In summary, the proposed controller improved both energy capture and tower fatigue loads as compared to the baseline controller. In our future work, the effect of imperfect preview of wind on the performance of eMPC will be investigated. Additionally, expanding the eMPC framework to mitigate the fatigue loads acting on the blades and the drivetrain will be addressed.

Funding Data

- Division of Civil, Mechanical and Manufacturing Innovation (Award No. CMMI-1056020).

Nomenclature

A = rotor swept area
B_s = drivetrain equivalent torsional damping
B_T = tower equivalent damping
c_p = power coefficient
c_t = thrust coefficient
D_r = rotor diameter
F_T = rotor thrust force
H_h = hub height
J = equivalent drivetrain moment of inertia
J_g = generator moment of inertia
J_r = rotor moment of inertia
K = kinetic energy stored in the rotating components
K_s = drivetrain equivalent torsional stiffness
K_T = tower equivalent stiffness
M_T = tower equivalent mass
n = gearbox ratio
N_p = prediction and control horizon
P_{av} = available wind power
P_g = generator power
P_r = rotor power
T_g = generator torque
T_r = rotor torque
v = wind speed
V = transformed fore-aft velocity of the tower top
X = transformed fore-aft displacement of the tower top
x_T = fore-aft displacement of the tower top
β = collective blade pitch angle
η_g = generator efficiency
λ = tip-speed ratio

ρ = air density
ϕ = drivetrain torsional deflection
ω_g = generator angular speed
ω_r = rotor angular speed

References

[1] Gelman, R., Meshek, M., Buchanan, S., and Augustine, E., 2013, "2012 Renewable Energy Data Book," National Renewable Energy Laboratory, Golden, CO, Report.
[2] Wiser, R., Bolinger, M., Barbose, G., Darghouth, N., Hoen, B., Mills, A., Weaver, S., Porter, K., Buckley, M., Oteri, F., and Tegen, S., 2014, "2013 Wind Technologies Market Report," U.S. Department of Energy, Oak Ridge, TN, Report No. DOE/GO-102014-4459.
[3] Lindenberg, S., Smith, B., O'Dell, K., DeMeo, E., and Ram, B., 2008, "20% Windpower by 2030," U.S. Department of Energy, Oak Ridge, TN, Report No. DOE/GO-102008-2578.
[4] Laks, J. H., Pao, L. Y., and Wright, A. D., 2009, "Control of Wind Turbines: Past, Present, and Future," American Control Conference (ACC), St. Louis, MO, June 10–12, pp. 2096–2103.
[5] Pao, L. Y., and Johnson, K. E., 2011, "Control of Wind Turbines: Approaches, Challenges, and Recent Developments," Control Syst. IEEE, **31**(2), pp. 44–62.
[6] García, C. E., Prett, D. M., and Morari, M., 1989, "Model Predictive Control: Theory and Practice—A Survey," Automatica, **25**(3), pp. 335–348.
[7] Qin, S. J., and Badgwell, T. A., 2003, "A Survey of Industrial Model Predictive Control Technology," Control Eng. Pract., **11**(7), pp. 733–764.
[8] Rawlings, J. B., 2000, "Tutorial Overview of Model Predictive Control," IEEE Control Syst. Mag., **20**(3), pp. 38–52.
[9] Yang, Z., Li, Y., and Seem, J. E., 2012, "Model Predictive Control for Wind Turbine Load Reduction Under Wake Meandering of Upstream Wind Turbines," American Control Conference (ACC), Montreal, QC, Canada, June 27–29, pp. 3008–3013.
[10] Khalid, M., and Savkin, A. V., 2010, "A Model Predictive Control Approach to the Problem of Wind Power Smoothing With Controlled Battery Storage," Renewable Energy, **35**(7), pp. 1520–1526.
[11] Rawlings, J. B., Angeli, D., and Bates, C. N., 2012, "Fundamentals of Economic Model Predictive Control," 51st IEEE Conference on Decision and Control (CDC), Maui, HI, Dec. 10–13, pp. 3851–3861.
[12] Grüne, L., 2013, "Economic Receding Horizon Control Without Terminal Constraints," Automatica, **49**(3), pp. 725–734.
[13] Diehl, M., Amrit, R., and Rawlings, J. B., 2011, "A Lyapunov Function for Economic Optimizing Model Predictive Control," IEEE Trans. Autom. Control, **56**(3), pp. 703–707.
[14] Angeli, D., Amrit, R., and Rawlings, J. B., 2012, "On Average Performance and Stability of Economic Model Predictive Control," IEEE Trans. Autom. Control, **57**(7), pp. 1615–1626.
[15] Rawlings, J. B., and Amrit, R., 2009, "Optimizing Process Economic Performance Using Model Predictive Control," *Nonlinear Model Predictive Control*, Springer, Berlin.
[16] Hovgaard, T. G., Edlund, K., and Jorgensen, J. B., 2010, "The Potential of Economic MPC for Power Management," 49th IEEE Conference on Decision and Control (CDC), Atlanta, GA, Dec. 15–17, pp. 7533–7538.
[17] Halvgaard, R., Poulsen, N. N. K., Madsen, H., and Jorgensen, J. B., 2012, "Economic Model Predictive Control for Building Climate Control in a Smart Grid," IEEE PES Innovative Smart Grid Technologies (ISGT), Washington, DC, Jan. 16–20, pp. 1–6.
[18] Hovgaard, T. G., Larsen, L. F. S., Jorgensen, J. B., and Boyd, S., 2013, "MPC for Wind Power Gradients—Utilizing Forecasts, Rotor Inertia, and Central Energy Storage," European Control Conference (ECC), Zurich, Switzerland, July 17–19, pp. 4071–4076.
[19] Hovgaard, T. G., Boyd, S., and Jørgensen, J. B., 2015, "Model Predictive Control for Wind Power Gradients," Wind Energy, **18**(6), pp. 991–1006.
[20] Gros, S., 2013, "An Economic NMPC Formulation for Wind Turbine Control," 52nd IEEE Conference on Decision and Control (CDC), Florence, Italy, Dec. 10–13, pp. 1001–1006.
[21] Gros, S., Vukov, M., and Diehl, M., 2013, "A Real-Time MHE and NMPC Scheme for Wind Turbine Control," 52nd IEEE Conference on Decision and Control (CDC), Florence, Italy, Dec. 10–13, pp. 1007–1012.
[22] Shaltout, M. L., Ma, Z., and Chen, D., 2016, "An Economic Model Predictive Control Approach Using Convex Optimization for Wind Turbines," American Control Conference (ACC), Boston, MA, July 6–8, pp. 3176–3181.
[23] Schlipf, D., Schlipf, D. J., and Kühn, M., 2013, "Nonlinear Model Predictive Control of Wind Turbines Using LIDAR," Wind Energy, **16**(7), pp. 1107–1129.
[24] Schlipf, D., Pao, L. Y., and Po Wen, C., 2012, "Comparison of Feedforward and Model Predictive Control of Wind Turbines Using LIDAR," 51st IEEE Conference on Decision and Control (CDC), Maui, HI, Dec. 10–13, pp. 3050–3055.
[25] Soltani, M., Wisniewski, R., Brath, P., and Boyd, S., 2011, "Load Reduction of Wind Turbines Using Receding Horizon Control," IEEE International Conference on Control Applications (CCA), Denver, CO, Sept. 28–30, pp. 852–857.
[26] Schlipf, D., Grau, P., Raach, S., and Duraiski, R., 2014, "Comparison of Linear and Nonlinear Model Predictive Control of Wind Turbines Using LIDAR," American Control Conference (ACC), Portland, OR, June 4–6, pp. 3742–3747.
[27] Yang, Z., Li, Y., and Seem, J. E., 2012, "Load Reduction of Wind Turbines Under Wake Meandering With Model Predictive Control for Individual Pitching," AIAA Paper No. 2012-1150.
[28] Henriksen, L. C., Hansen, M. H., and Poulsen, N. K., 2012, "Wind Turbine Control With Constraint Handling: A Model Predictive Control Approach," IET Control Theory Appl., **6**(11), pp. 1722–1734.
[29] Gerber, B. S., Herr, S., and Pierce, K. G., 2012, "Variable Tip Speed Ratio Tracking Control for Wind Turbines," General Electric Company, Boston, MA, U.S. Patent No. US8215906 B2.
[30] Mirzaei, M., Poulsen, N. K., and Niemann, H. H., 2012, "Robust Model Predictive Control of a Wind Turbine," American Control Conference (ACC), Montreal, QC, Canada, June 27–29, pp. 4393–4398.
[31] Evans, M. A., Cannon, M., and Kouvaritakis, B., 2015, "Robust MPC Tower Damping for Variable Speed Wind Turbines," IEEE Trans. Control Syst. Technol., **23**(1), pp. 290–296.
[32] Johnson, K. E., Fingersh, L. J., Balas, M. J., and Pao, L. Y., 2004, "Methods for Increasing Region 2 Power Capture on a Variable-Speed Wind Turbine," ASME J. Sol. Energy Eng., **126**(4), pp. 1092–1100.
[33] Johnson, K. E., Pao, L. Y., Balas, M. J., and Fingersh, L. J., 2006, "Control of Variable-Speed Wind Turbines: Standard and Adaptive Techniques for Maximizing Energy Capture," IEEE Control Syst. Mag., **26**(3), pp. 70–81.
[34] Song, Y. D., Dhinakaran, B., and Bao, X. Y., 2000, "Variable Speed Control of Wind Turbines Using Nonlinear and Adaptive Algorithms," J. Wind Eng. Ind. Aerodyn., **85**(3), pp. 293–308.
[35] Freeman, J., and Balas, M., 1999, "An Investigation of Variable Speed Horizontal-Axis Wind Turbines Using Direct Model-Reference Adaptive Control," AIAA Paper No. 1999-0028.
[36] Ma, Z., Shaltout, M. L., and Chen, D., 2014, "Adaptive Gain Modified Optimal Torque Controller for Wind Turbine Partial Load Operation," ASME Paper No. DSCC2014-5921.
[37] Ma, Z., Shaltout, M. L., and Chen, D., 2015, "An Adaptive Wind Turbine Controller Considering Both the System Performance and Fatigue Loading," ASME J. Dyn. Syst. Meas. Control, **137**(11), p. 111007.
[38] Jonkman, J., Butterfield, S., Musial, W., and Scott, G., 2009, "Definition of a 5-MW Reference Wind Turbine for Offshore System Development," National Renewable Energy Laboratory, Golden, CO, Technical Report No. NREL/TP-500-38060.
[39] Grunnet, J. D., Soltani, M., Knudsen, T., Kragelund, M. N., and Bak, T., 2010, "Aeolus Toolbox for Dynamics Wind Farm Model, Simulation and Control," European Wind Energy Conference and Exhibition (EWEC), Warsaw, Poland, Apr. 20–23, pp. 3119–3129.
[40] Bottasso, C. L., Croce, A., Savini, B., Sirchi, W., and Trainelli, L., 2006, "Aero-Servo-Elastic Modeling and Control of Wind Turbines Using Finite-Element Multibody Procedures," Multibody Syst. Dyn., **16**(3), pp. 291–308.
[41] Magnani, A., and Boyd, S. P., 2009, "Convex Piecewise-Linear Fitting," Optim. Eng., **10**(1), pp. 1–17.
[42] Schlipf, D., Fleming, P., Kapp, S., Scholbrock, A., Haizmann, F., Belen, F., and Wright, A., 2013, "Direct Speed Control Using LIDAR and Turbine Data," American Control Conference (ACC), Washington, DC, June 17–19, pp. 2208–2213.
[43] Wang, N., Johnson, K. E., and Wright, A. D., 2013, "Comparison of Strategies for Enhancing Energy Capture and Reducing Loads Using LIDAR and Feedforward Control," IEEE Trans. Control Syst. Technol., **21**(4), pp. 1129–1142.
[44] Harris, M., Hand, M., and Wright, A., 2005, "Lidar for Turbine Control," National Renewable Energy Laboratory, Golden, CO, Technical Report No. NREL/TP-500-39154.
[45] Wang, N., Johnson, K. E., and Wright, A. D., 2012, "FX-RLS-Based Feedforward Control for LIDAR-Enabled Wind Turbine Load Mitigation," IEEE Trans. Control Syst. Technol., **20**(5), pp. 1212–1222.
[46] Dunne, F., Pao, L. Y., Wright, A. D., Jonkman, B., and Kelley, N., 2011, "Adding Feedforward Blade Pitch Control to Standard Feedback Controllers for Load Mitigation in Wind Turbines," Mechatronics, **21**(4), pp. 682–690.
[47] Zhang, Y., Cheng, M., and Chen, Z., 2013, "Proportional Resonant Individual Pitch Control for Mitigation of Wind Turbines Loads," IET Renewable Power Gener., **7**(3), pp. 191–200.
[48] Hayman, G., and Buhl, M., 2012, "MLife User's Guide," National Renewable Energy Laboratory, Golden, CO, Technical Report.
[49] Jonkman, B. J., 2009, "TurbSim User's Guide: Version 1.50," National Renewable Energy Laboratory, Golden, CO, Technical Report No. NREL/TP-500-46198.